Author's personal copy

Journal of Structural Geology 30 (2008) 839–853

Contents lists available at ScienceDirect

Journal of Structural Geology

journal homepage: www.elsevier.com/locate/jsg

Oblique half-graben inversion of the Mesozoic Neuquén Rift in the Malargüe Fold and Thrust Belt, Mendoza, Argentina: New insights from analogue models

Daniel L. Yagupsky [a,*], Ernesto O. Cristallini [a], Julián Fantín [b], Gonzalo Zamora Valcarce [b], Germán Bottesi [c], Roberto Varadé [c]

[a] Laboratorio de Modelado Geológico (LaMoGe), Universidad de Buenos Aires, Ciudad Universitaria, C1428EHA, Buenos Aires, Argentina, and Consejo Nacional de Investigaciones Científicas y Técnicas (CONICET), Avda. Rivadavia 1917, CP C1033AAJ, Ciudad de Buenos Aires, Argentina
[b] Repsol YPF S.A. Talero 360, 8300 Neuquén, Argentina
[c] Repsol YPF, Esmeralda 255, piso 10, Of. 10001E, Buenos Aires, Argentina

ARTICLE INFO

Article history:
Received 14 August 2007
Received in revised form 4 March 2008
Accepted 27 March 2008
Available online 8 April 2008

Keywords:
Analogue modeling
Oblique inversion
Malargüe fold
Thrust belt

ABSTRACT

The Malargüe fold and thrust belt, located in the Andean mountains between 34°S and 36°30′S, formed in response to contraction during Cenozoic times. Its structural style and geometry was controlled by the Mesozoic rift system that formed the Neuquén basin in west-central Argentina. The rift architecture in the southern sector of this belt was previously interpreted in terms of the present N–S compressive structural trends, assuming the inversion of pre-existing normal faults with the same orientation. Here, we propose that the NW–SE-trending El Manzano–Liu Cullín lineament, located in the northern termination of the Sierra Azul, reflects the presence of a half-graben master fault in the subsurface. This hypothesis is supported by subsurface data, a balanced cross section, and it is tested using a series of scaled sandbox analogue models. We suggest that the lineament responds to a reactivated NW-trending half-graben fault, hidden by the mainly N–S-trending Andean structures. The proposed orientation is in agreement with the NE–SW extension developed in the Neuquén basin during the Triassic–Early Jurassic. The modeling of the inverted oblique half-graben reveals that the strikes of the main structures of inversion-related belts may often be independent of the orientation of the previously developed extensional system, providing a new perspective for their interpretation.

© 2008 Published by Elsevier Ltd.

1. Introduction

The Malargüe fold and thrust belt (Fig. 1) is a Cenozoic thick-skinned deformational system controlled by previously developed extensional structures (Kozlowski et al., 1993; Manceda and Figueroa, 1993, 1995; Mingramm et al., 1993; Dimieri, 1997; Silvestro and Kraemer, 2005). Based on subsurface data, Manceda and Figueroa (1993, 1995) described the main structures for the southern sector of this belt as being controlled by Jurassic rift infrastructure. Transverse lineaments were interpreted as accommodation zones and transfer faults related to the rift phase. However, despite the amount of work done in the area (Groeber, 1937; Dessanti, 1973; Legarreta et al., 1985; Kozlowski et al., 1989; Gulisano and Gutierrez Pleimling, 1994), the origin of the oblique structures developed across the Malargüe fold and thrust belt is still problematic, masked by the sparse subsurface data, and by the few exposures of the syn-rift deposits.

The origin of oblique structures in fold and thrust belts has been related to a number of factors, including positive inversion of pre-existing extensional structures (Gillcrist et al., 1987; Vergés and Muñoz, 1990; Burbank et al., 1992; Casas-Sainz, 1993; Carrera et al., 2006), oblique and lateral ramps in the sole thrust (e.g. Macedo and Marshak, 1999) or folding interference patterns (Carrera et al., 2006). Furthermore, studies performed in the NW Argentinean Andes suggest that certain structures departing from the N–S regional trend developed in the early stages of the oblique inversion process: as deformation progressed, reactivation of the extensional faults became less important and N–S trending thrust and folds dominated (Carrera et al., 2006). To address the occurrence of this kind of geometric control, a complete understanding of the underlying structure is needed. However, the quality of seismic imaging deteriorates significantly beneath deformed areas, obstructing the interpretation of the deeper level structural architecture.

Analogue modeling provides an opportunity to better understand the geometries and evolution of inversion systems. In this paper we perform analogue experiments to simulate the inversion

* Corresponding author. Laboratorio de Modelado Geológico (LaMoGe), Universidad de Buenos Aires, Ciudad Universitaria, C1428EHA Buenos Aires, Argentina. Fax: +54 11 4576 3329.
E-mail address: daniely@gl.fcen.uba.ar (D.L. Yagupsky).

0191-8141/$ – see front matter © 2008 Published by Elsevier Ltd.
doi:10.1016/j.jsg.2008.03.007

Author's personal copy

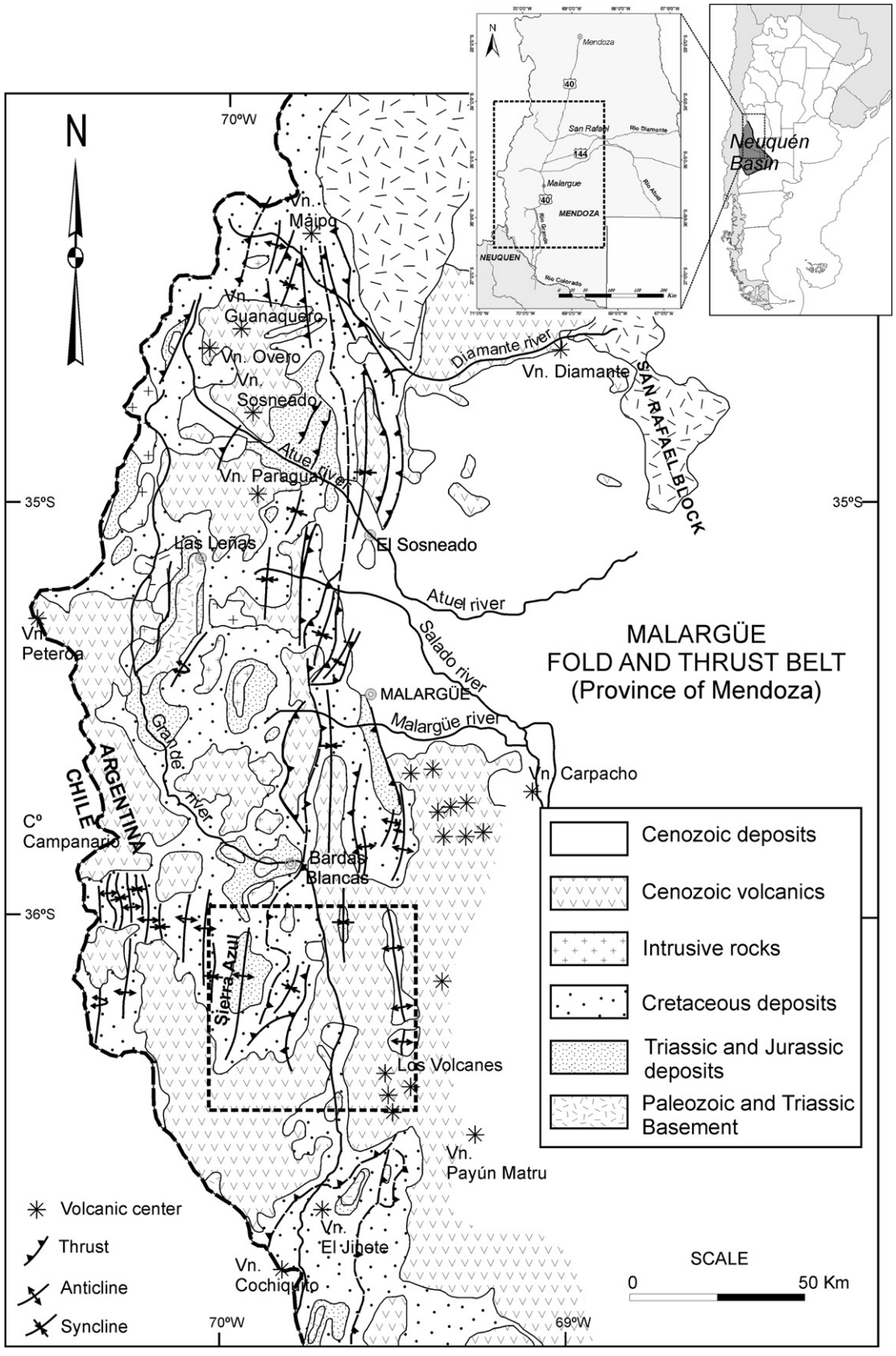

Fig. 1. Geographical and geological settings of the study area (map modified from Kozlowski et al., 1993). The section of the thick-skinned Malargüe fold and thrust belt considered in this study is shown in the boxed region.

Author's personal copy

of rift structures with different obliquity between the direction of contraction and normal faults. Comparison of the experimental results with field and reflection seismic data from the Malargüe fold and thrust belt allows us to hypothesize about the origin of oblique structures in this region. We evaluate the possibility that the El Manzano–Liu Cullín lineament, located in the northern termination of the Sierra Azul (Fig. 2), reflects the presence of an oblique reactivated NW-trending and SW-dipping half-graben fault, hidden by the mainly N–S-trending Andean structures. This comparison permits a structural explanation of the observed geometries, and provides a suitable progressive model for the inversion process that is also applicable to other inversion-related regions.

2. Geological setting

The Malargüe fold and thrust belt, south of Rio Diamante (Fig. 1), is a Cenozoic deformational system that results from the interaction of Andean contractional deformation with pre-existing extensional basin structures (Kozlowski et al., 1993). The oldest rocks that crop out are a suite of Permo-Triassic volcanics, the Choiyoi Group, with an unexposed base in this region. The Choiyoi are rhyolitic–dacitic rocks with some intercalated clastics, overlain by a Mesozoic sequence composed of marine sedimentary rocks and continental units (Fig. 3). Tertiary molasse sequences cover the Mesozoic strata to the east of Sierra Azul. Laccolithic and sill-like Tertiary intrusives, as well as extrusive units, are widespread along the length of the mountain front (Groeber, 1980).

Due to tectonic extension related with the fragmentation of Gondwana and the opening of the South Atlantic Ocean (Dalziel, 1986; Uliana et al., 1989) during the Late Triassic–Early Jurassic, the Neuquén Basin experienced a main pulse of extensional deformation that mostly reactivated Paleozoic structural fabrics (Dalziel, 1986; Ramos, 1989; Uliana et al., 1989). The active rifting that affected the Permo-Triassic Choiyoi basement produced the

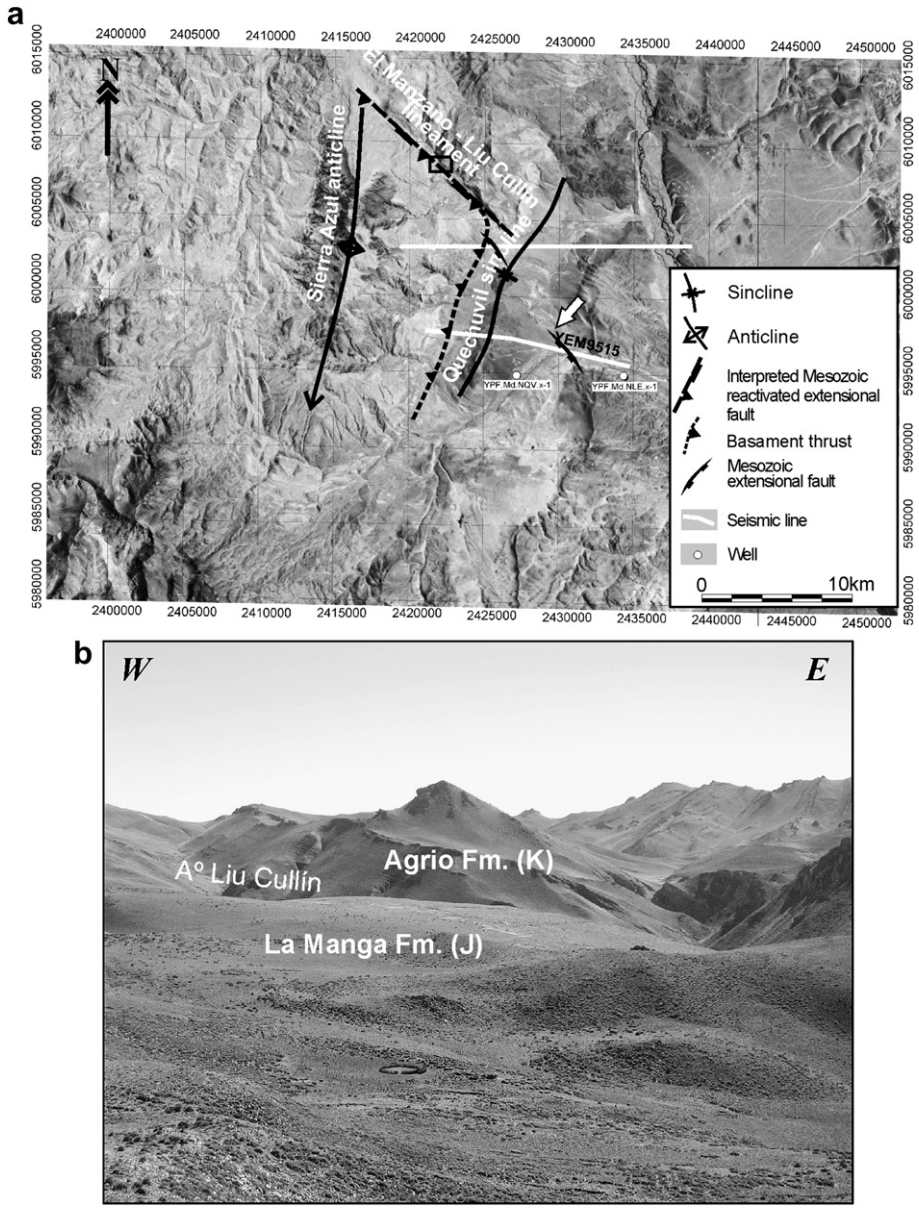

Fig. 2. (a) Thematic mapper image of the Sierra Azul showing the main structures of the region (location in Fig. 1). The arrow indicates the interpreted normal fault shown in the seismic section of Fig. 6. (b) View to the north of the lineament zone, with the Oxfordian limestones of La Manga Formation to the south and the Valanginian shales of Agrio Formation to the north.

Author's personal copy

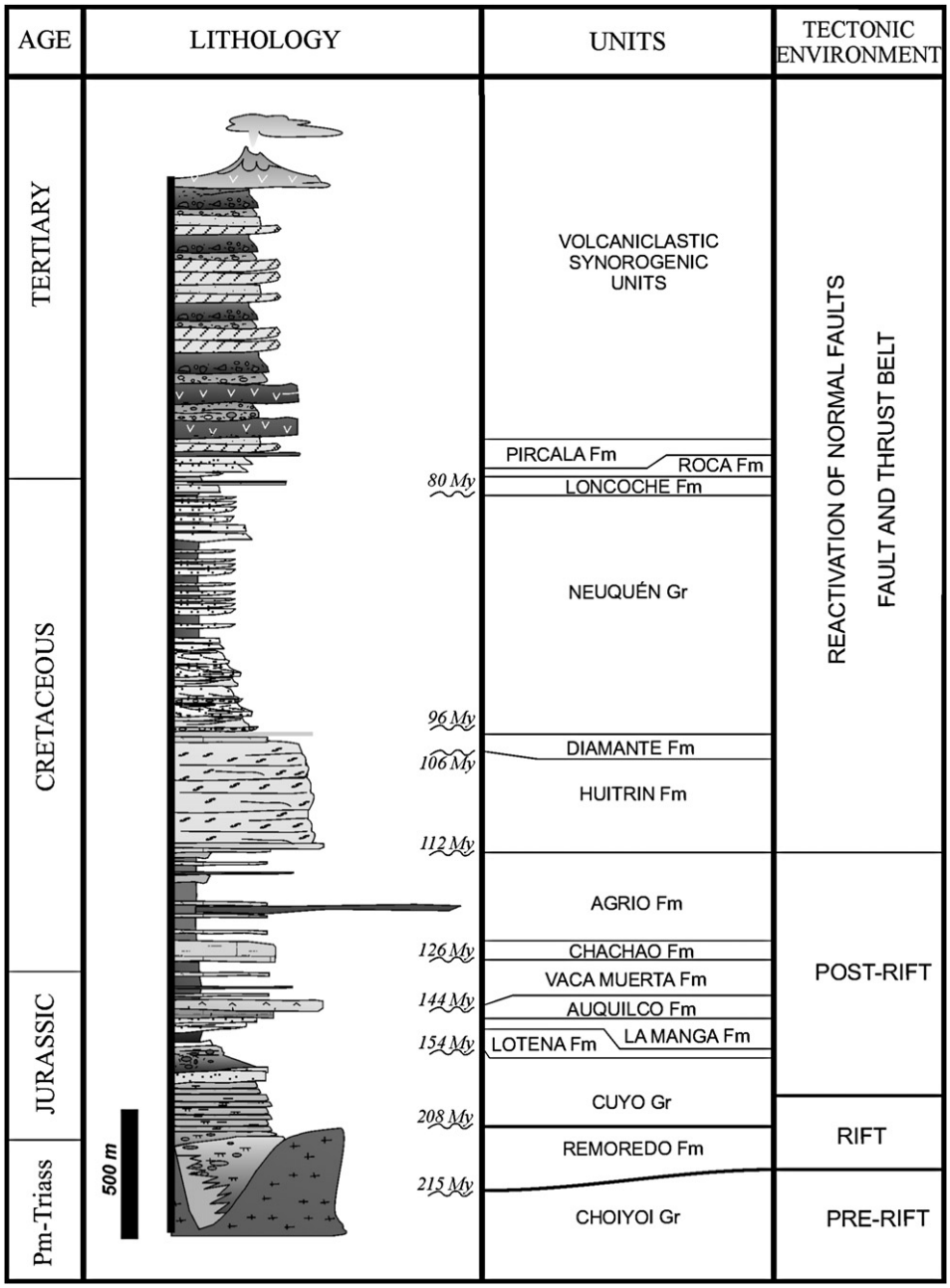

Fig. 3. Stratigraphic column showing the main lithologic units in the region, modified from Brissón and Veiga (1998).

coarse-grained Remoredo Formation of pre-Cuyo Group, and the lowermost units of Cuyo Group (Fig. 3; Manceda and Figueroa, 1993, 1995). Mesozoic rift-related depocenters of the northern Malargüe fold and thrust belt (Atuel depocenter; Fig. 1) were controlled by NNW-trending border faults (Alvarez et al., 2000; Giambiagi et al., 2005). To the south, in the region studied in this paper (Fig. 1), a north–south half-graben orientation was inferred from the available subsurface data, and from present north–south structural trends (Manceda and Figueroa, 1993, 1995). Additionally, ENE and ESE trending normal faults without evidence of inversion were found in both the Sierra de Cara Cura, and in the Sierra de Reyes, to the south of the Payún Matru volcano (Pángaro et al., 2004). Regionally, seismic data show that the half-grabens subsided along boundary faults of various orientations (Uliana et al., 1989).

Fault-controlled subsidence decreased up to the late Toarcian, when a general period of thermal subsidence began (Fig. 3). During this more regional pattern of subsidence, various sparse depocenters were linked, as the retroarc Neuquén basin developed (Legarreta and Gulisano, 1989; Legarreta and Uliana, 1991; Vergani et al., 1995). Nevertheless, irregular topography persisted locally, especially adjacent to the principal faults controlling the distribution of the Jurassic megasequences (Manceda and Figueroa, 1993).

Some of the master faults of the half-grabens were reactivated and inverted during the Andean contraction. The amount of shortening in this area averages ~30% (Manceda and Figueroa, 1993). Changes in structural style and vergence along strike were interpreted to be controlled by the initial extensional fault system (Fig. 1; Manceda and Figueroa, 1995, Fig. 9). The Permo-Triassic basement is involved in the deformation in the hinterland, as well as in the foothills adjacent to the foreland areas.

Cenozoic tectonic activity was episodic and discontinuous, as recorded by the synorogenic deposits close to the city of Malargüe

Author's personal copy

(Silvestro and Kraemer, 2005). Radiometric dating of andesitic lavas and basalts intercalated in the growth sequence constrain the age of deformation, recording two in-sequence pulses of foreland fold belt migration during Middle–Upper Miocene and Pliocene time respectively. At the end of the second pulse, the deformation shifted toward the hinterland; in this sector of the belt Pleistocene strata buried the Pliocene deformation front (Silvestro and Kraemer, 2005).

3. El Manzano–Liu Cullín lineament

3.1. Surface data

The El Manzano–Liu Cullín lineament is located at the northern edge of the Sierra Azul, to the south of the Malargüe fold and thrust belt (Fig. 2). Its morphological expression consists of a deep NW-trending valley that puts the Oxfordian marine platform limestones of La Manga Formation to the south, in lateral contact with the Valanginian platform sediments of the Agrio Formation (Mendoza Group) to the north (Figs. 2 and 4).

The thickness of the pre-Cuyo Group (Remoredo Formation) to the south of the lineament is more than 200 m with an unexposed base, while to the north, in the Bardas Blancas section, it is only 60 m thick (Fig. 5).

3.2. Subsurface data

Using 2D seismic data, three high angle normal faults dipping to the west, and affecting the structural basement (Choiyoi Group), have been imaged along the eastern edge of the Sierra Azul (Fig. 6). These faults bound wedge-shaped groups of well-defined seismic reflectors interpreted as a sequence of syn-rift half-graben fill (pre-Cuyo Group, and the lowermost units of Cuyo Group) with no evidence of tectonic inversion. Beneath this sequence, the seismic signal is less defined, forming a seismic unit that is interpreted as Choiyoi Group volcanics. Using this seismic line, exploration wells and surface data, a balanced cross section was prepared (Fig. 7b).

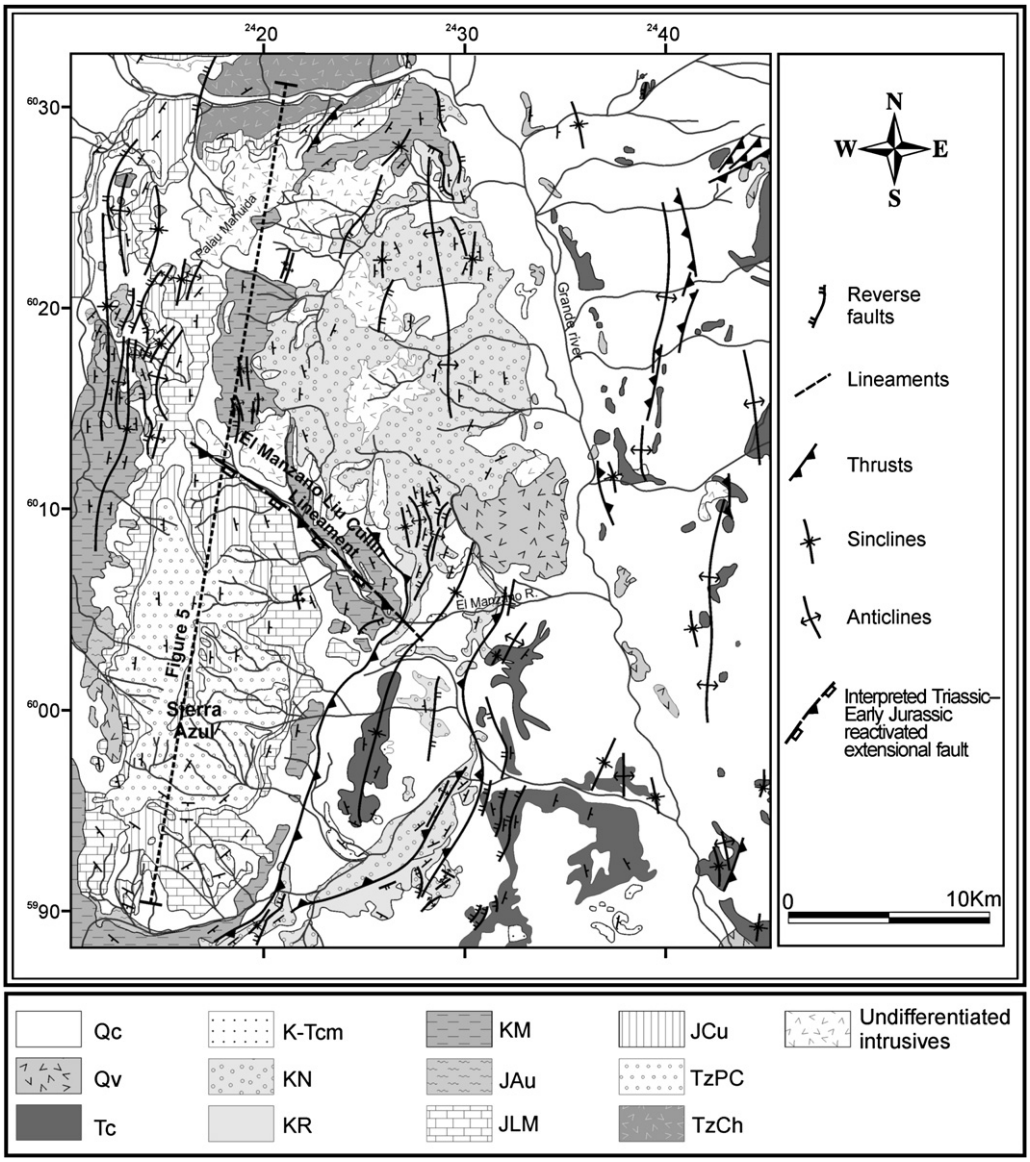

Fig. 4. Geologic map of Sierra Azul and western Sierra de Palauco region, modified from Groeber, 1937; Dessanti, 1973; Legarreta et al., 1985; Kozlowski et al., 1989; Gulisano and Gutierrez Pleimling, 1994; Dicarlo, 2005. Qc, clastic Quaternary; Qv, volcanic Quaternary; Tc, Tertiary; K–Tcm, Malargüe Group; KN, Neuquén Group; KR, Rayoso Group; KM, Mendoza Group; JAu, Auquilco Formation; JLM, La Manga Formation; JCu, Cuyo Group; TzPC, pre-Cuyo Group; TzCh, Choiyoi Group.

Author's personal copy

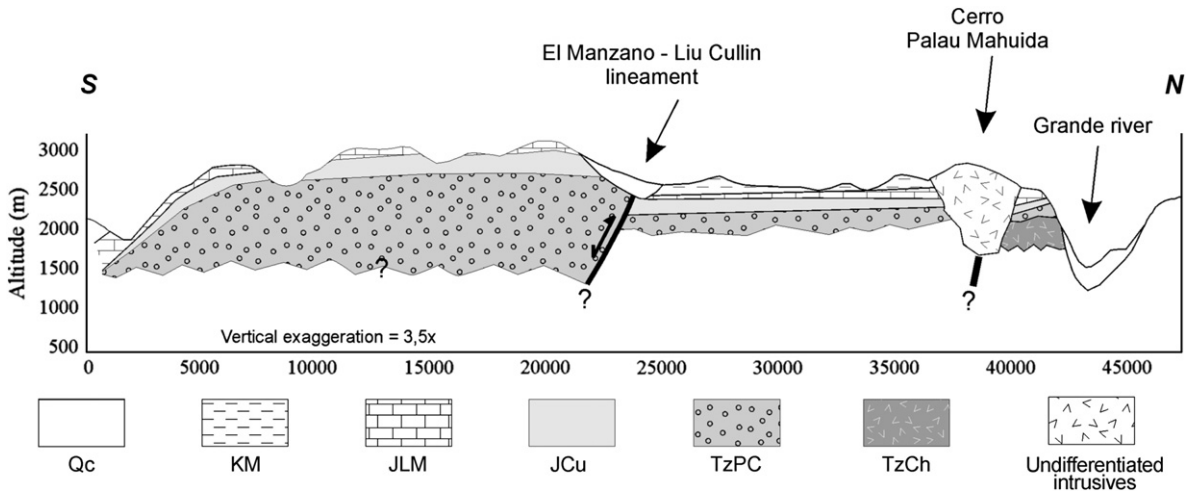

Fig. 5. Schematic north–south cross section of the Sierra Azul (see Fig. 4 for location), showing the difference in structural height between the north and the south of the lineament. Qc, clastic; KM, Mendoza Group; JLM, La Manga Formation; JCu, Cuyo Group; TzPC, pre-Cuyo Group; TzCh, Choiyoi Group. Vertical exaggeration = 3.5×.

Another west-dipping half-graben bounding fault without reactivation evidences has been interpreted in the front of Sierra Azul using well information and 2D seismic data (location in Fig. 7a; seismic reflection profile is not shown for reasons of confidentiality, see Quintana, 2008). The identified structure affects the basement and bounds Jurassic sequences of pre-Cuyo Group.

3.3. Surface and subsurface integration

Two Mesozoic normal faults are indicated in the structural section, and in the map of Fig. 7. The roughly NNE-trending thrust front of the Sierra Azul marks the eastern limit of the area with basement-involved deformation (Fig. 7a). Fig. 8b shows the palinspastically restored cross section of Fig. 7b, depicting a shortening of 4.2 km (22.25%) for the Mendoza Group (Fantín, 2006). Using this amount of E–W shortening we constructed a palinspastic map showing the pre-contraction location of the El Manzano–Liu Cullín lineament (Fig. 8a). A perfect alignment with the two highlighted normal faults identified by subsurface data can be seen, suggesting that they may have been segments of a single structure prior to Andean deformation.

4. Analogue modeling

A number of analogue modeling studies have investigated the effects of "inversion": that is, rift basin development followed by contractional deformation (e.g., Koopman et al., 1987; McClay, 1989; Buchanan and McClay, 1991, 1992; McClay and Buchanan, 1992; Mitra and Islam, 1994; Eisenstadt and Withjack, 1995; Brun and Nalpas, 1996; McClay et al., 2000; Dubois et al., 2002; Amilibia et al., 2005; Panien et al., 2005; Del Ventisette et al., 2006). In particular, Brun and Nalpas (1996), Panien et al. (2005) and Del Ventisette et al. (2006) successfully simulated the inversion of extensional structures with oblique initial basin orientation.

Here, we conducted sandbox analogue experiments to test the influence on tectonic inversion of half-grabens oblique to the

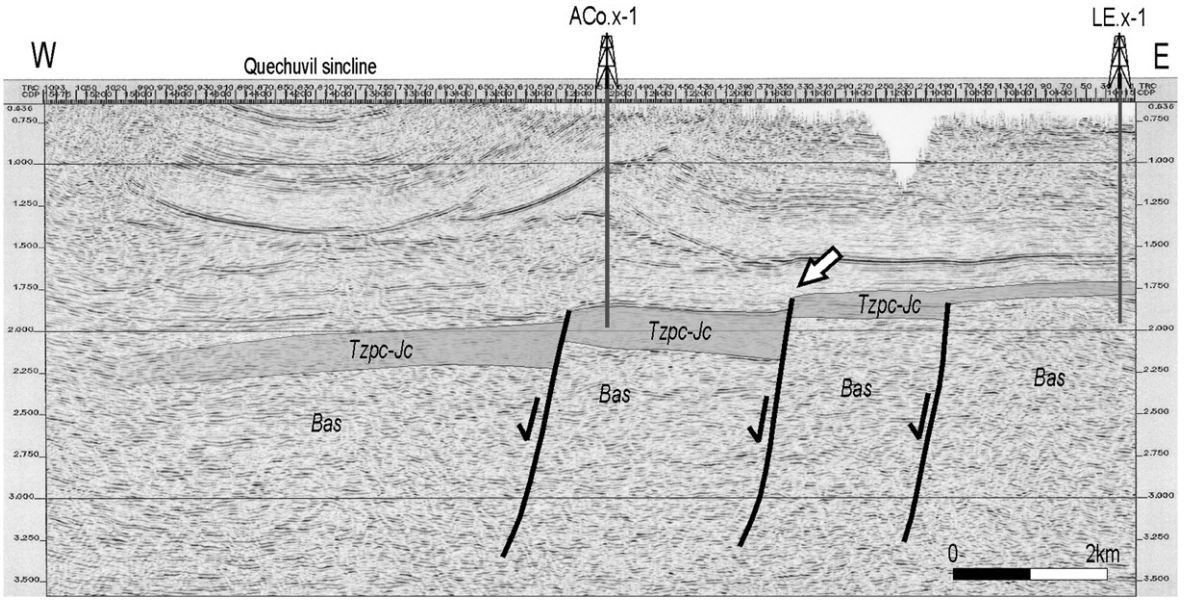

Fig. 6. Seismic line used to build the structural section in Fig. 7b. The arrow indicates the normal fault highlighted in Fig. 2. Bas, basement of the Mesozoic succession (Choiyoi Group); Tzpc, pre-Cuyo Group; Jc, Cuyo Group. ACo.x-1: Arroyo Coehueco x-1. LE.x-1: Loma de las Espinas x-1. See Fig. 2 for location.

Author's personal copy

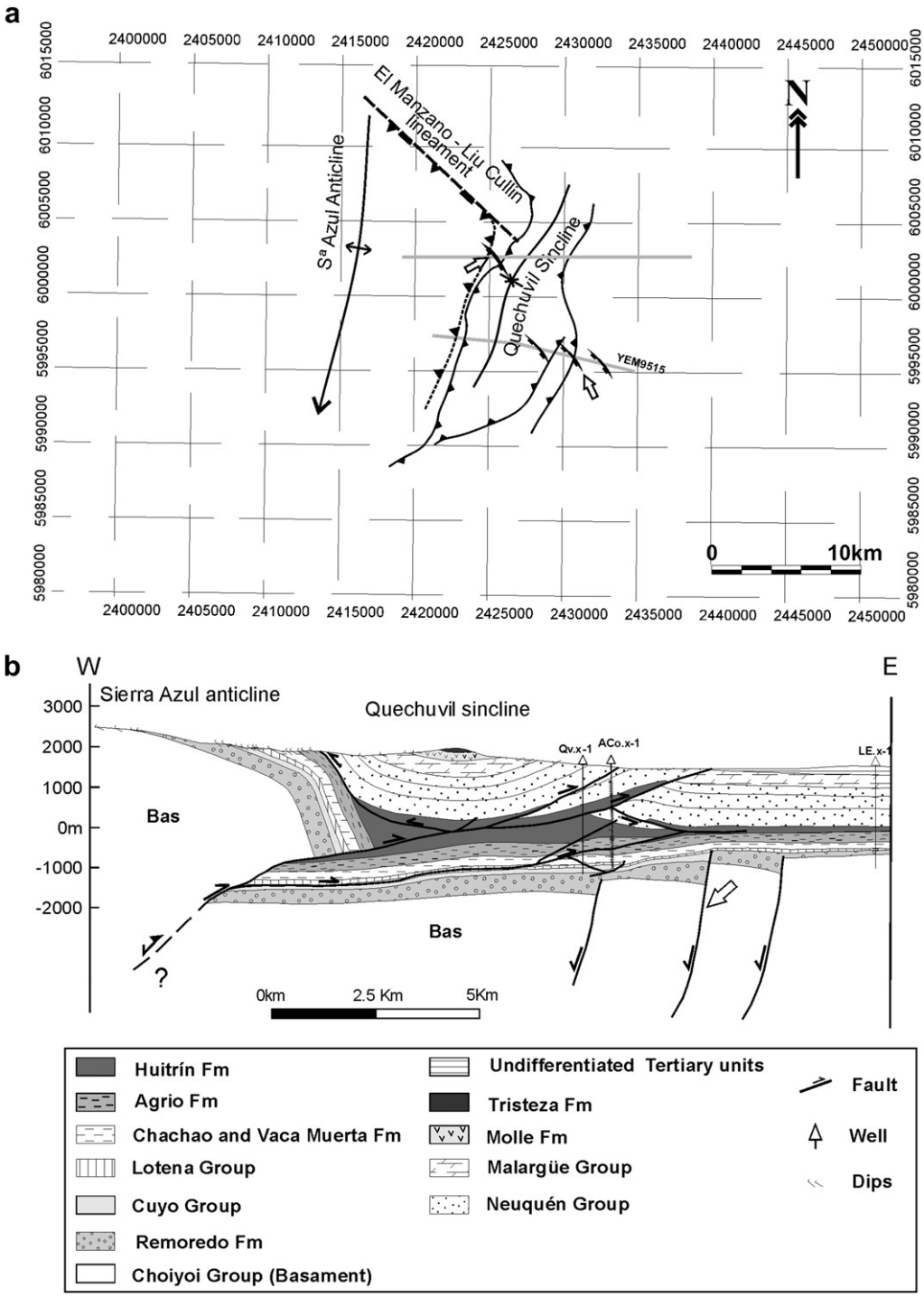

Fig. 7. (a) Main structural features of the Sierra Azul area. The arrows highlight the basement normal faults identified in Fig. 6 and panel b, and discussed in the text. References in Fig. 2. (b) Balanced cross section based on seismic line of Fig. 6, between the eastern flank of the Sierra Azul and the Arroyo Mechanquil.

shortening direction. The main objective of the simulations was to investigate the evolution of the oblique inversion process, and to contrast the results with the working hypothesis suggested by our field and geophysical data in the southern Malargüe fold and thrust belt.

4.1. Experimental method

The model materials were well sorted dry quartz sand with well rounded grains smaller than 600 μm, and glass microbeads. To a first approximation, such materials fail according to a linear Mohr envelope (Krantz, 1991). Their mechanical properties were measured with a modified Hubbert-type shear apparatus (Hubbert, 1951), which enables the determination of the ratio of normal-to-shear stress at failure. The coefficient of friction and the cohesion were then determined by linear regression analysis (Fig. 9). The test results indicated that the quartz sand has a friction angle of ~32.7°, similar to the values determined experimentally for competent upper crustal rocks (Byerlee, 1978). Microbeads, with a friction angle of ~28.3°, are much weaker and were used to simulate less

Author's personal copy

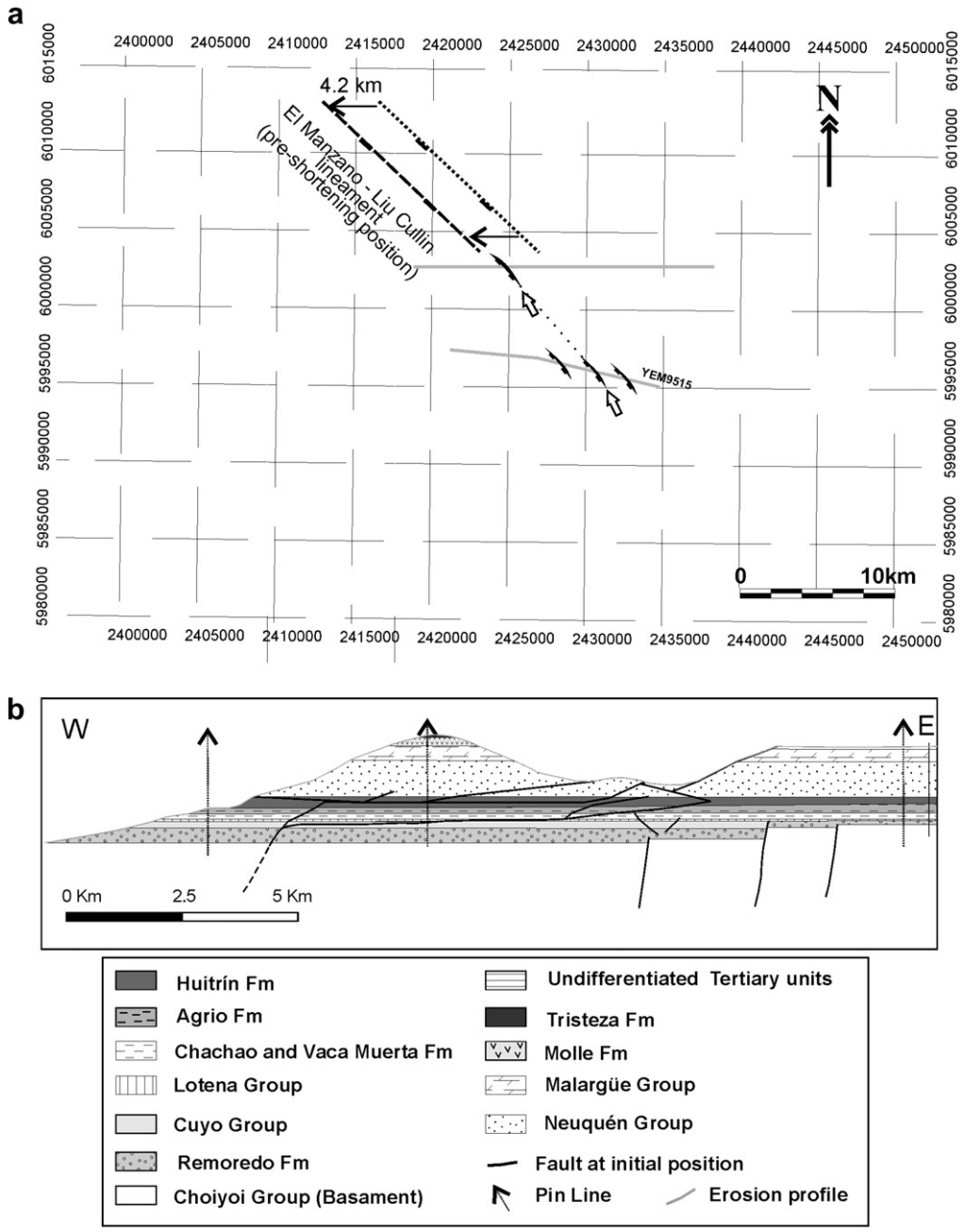

Fig. 8. (a) Palinspastically restored map of Fig. 7a in accordance with the 4.2 km of shortening calculated. The arrows highlight the basement normal faults aligned with the restored position of the El Manzano–Liu Cullin lineament. (b) Palinspastically restored cross section of Fig. 7b.

competent rocks. The basal friction (μ_b) between granular materials and the plastic sheet of the basal interface is low ($\mu_b = 0.16 \pm 0.02$), in agreement with an effective decollement in the upper crust. Standard error for the coefficient of friction was smaller than 0.06 (Fig. 9). Cohesion cannot be determined accurately with this method. However, this parameter was very low (<100 Pa; Fig. 9) when compared with normal stress acting in the sandbox experiments (>1000 Pa). Thus these materials are good analogues for simulating brittle deformation in the uppermost crust (Hubbert, 1937, 1951; Sandford, 1959) assuming time independent rheological behavior.

Analogue experiments must be scaled in order to get geometric, kinematic and dynamic similarities with the natural examples they represent (Hubbert, 1937; Ramberg, 1981). The models described in this paper are scaled such that 1 cm in the model simulates approximately 1 km in the field (geometric scale factor $\lambda = 10^{-5}$); the density ratio (ρ) between the used granular materials and rocks is $\rho \approx 0.5$, while both the prototype and the model are subject to the same value of gravitational acceleration, imposing a scale factor $g = 1$. The stress scale factor σ is given by:

$$\sigma = \rho \cdot g \cdot \lambda \approx 5 \times 10^{-6}$$

Assuming a Coulomb behavior for the upper crust rocks and a mean value of cohesion $C \approx 10^7$ Pa, the analogue granular materials, with, with $C \sim$ 10–30 Pa, are appropriate for working at the selected scale.

Three experiments were performed to test the influence of the orientation of the half-graben with respect to the shortening direction on the resulting structures. Each was run twice to ensure reproducibility. The models contained alternating layers of sieved

Author's personal copy

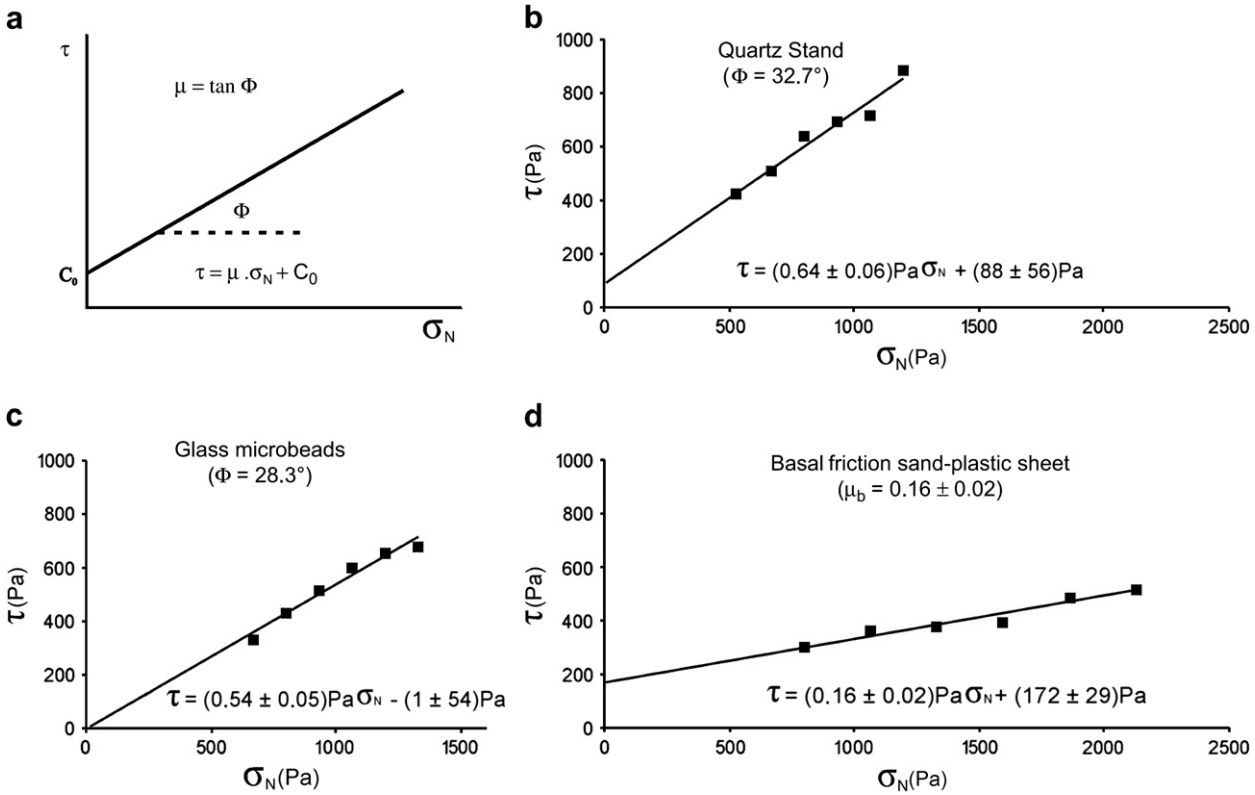

Fig. 9. Shear stress (τ) plotted as a function of normal stress (σ_N) for tested materials in the Hubbert-type shear box. (a) The slope gradient of the line represents the friction angle (Φ); the intersection of the line with the ordinate represents the cohesion (C_0); μ, coefficient of friction. (b–d) Internal friction, friction angle and basal friction (μ_b) for the materials used in the models derived from linear regression analyses.

light and dark quartz sand, each 0.3 cm thick. The sand layers overlaid two plastic sheets that generated a basal discontinuity (Fig. 10). The undeformed multilayers were 35 cm long, 39 cm wide and 2 cm thick. The extensional stage was achieved by moving one of the basal sheets away from the other. The sand part covering the mobile plastic sheet was carried 2 cm away at a rate of 6 cm/h, whereas the other part did not move. Between these two parts, a slightly asymmetric graben with a geometry quite close to that of a half-graben was created. In all experiments this first extensional phase was identical in terms of bulk extension and velocity. The initial half-graben orientation was varied by changing the geometry of the basal plastic sheet (Fig. 10).

Accommodation space generated by extension (~1 cm deep) was filled with glass microbeads. Then, a post-rift 1 cm thick sand package was added over the models, composed again of alternating layers of light and dark colored quartz sand. The final thickness of the models was 3 cm (Fig. 11).

During the latter deformation phase the three models were shortened, displacing a moving wall at a constant rate of 6 cm/h. The angles α between the moving wall and the trend of the main normal faults were 15°, 30° and 45°, respectively (Fig. 10). The top surfaces of each experiment were recorded every minute using digital photography. The completed models were solidified, serially sectioned perpendicularly to the mobile wall, and scanned in order to determine their 3D structure. As a reference system, the contractional front advancing from west to east was chosen.

4.2. Model results

4.2.1. Extensional deformation stage

During the extensional stage a roughly asymmetric half-graben developed in all the models (Fig. 11). The structural configuration obtained was relatively simple and similar in all three experiments. The layers situated over the edge of the fixed plastic sheet slid down a master fault plane dipping 40° to the NE. The mobile part moved away from the fixed one, developing a conjugated major fault dipping between 40 and 45° to the SW; a few synthetic and

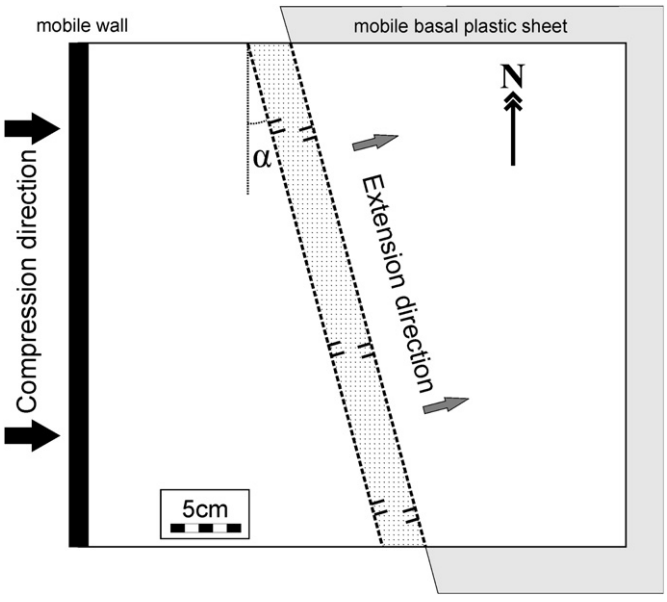

Fig. 10. Experimental set-up, showing a plan view of the basal plate configuration. Oblique half-graben developed after 2 cm of extension. Obliquity angles α of 15°, 30° and 45° were performed in models 1, 2 and 3, respectively.

Author's personal copy

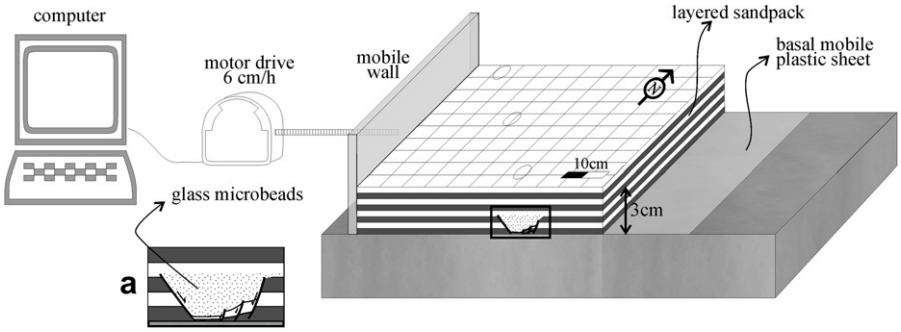

Fig. 11. Drawing of the experimental apparatus, showing a cross sectional view of the model after 2 cm of extension. Inset (a) shows a zoom of the half-graben outlined in the block diagram.

antithetic minors faults were formed in its hanging wall. This pattern persisted along the strike of the half-graben, without substantial differences. In each experiment the orientation of the axis of the extensional system was modified by changing the displacement direction applied (Fig. 10).

4.2.2. Contractional deformation stage. Model 3 ($\alpha = 45°$)

The contractional stage of model 3 can be summarized in the 6 pictures shown in Fig. 12. Fig. 12A displays the initial configuration of the experiment. In the following step (Fig. 12B), a N–S-trending thrust and backthrust can be observed. In the southern part of the model an inflexion developed, likely due to imperfect initial topography.

With increased shortening (2.5 cm), a thrust and backthrust developed (Fig. 12C). This "pop-up" structure had a northwest-trending axis following the pre-existing rift border faults, creating an active deformation front oblique to the one developed in the previous stage. The faults did not grow simultaneously throughout the whole model, but first they initiated in its northwestern portion, where the half-graben was closest to the mobile wall, and during further shortening they propagated laterally. Both deformation fronts were simultaneously active, although the oblique front was confined to the northwest of the model.

In the next stage (Fig. 12D), the reactivated sector of the half-graben was faulted by a thrust. A conjugate backthrust also developed. The new thrust branched from the previously developed oblique one, creating a new active deformation front in the inner side of the system. Its trace departed from the underlying structure in the north of the model. After a slight recess towards the hinterland across the preceding "pop-up" structure, it propagated to the south perpendicular to the shortening direction (roughly N–S). Both the NW–SE and the N–S fronts remained simultaneously active.

At the next stage of shortening (Fig. 12E) the NW-trending thrust and backthrust propagated to the SE, following the underlying structure geometry. After 7.5 cm of shortening (stage F), both advancing structures departed from the pre-existing extensional system, following a N–S strike towards the southern half of the model. The final map pattern records only one active deformation front with a significant change in strike in the north.

Both deformation style and evolution during shortening were quite similar for stages C–D and E–F (Fig. 12). The oblique half-graben-bounding faults were partially reactivated only at the sector closest to the advancing deformation front, propagating laterally during further shortening. In this area, the emerging forethrust and backthrusts were oblique to the mobile wall, reflecting the initial position of the half-graben. When this mechanical control was no longer efficient, the reverse faults became parallel to the mobile wall (see also Yagupsky et al., 2007). The resulting structural architecture is displayed in Fig. 12D and F. It is noteworthy that the portion of the half-graben distal to the mobile wall is either not reactivated (Fig. 12F), or only partly so (Fig. 12D), while the portion that is closest to the wall is reactivated and transported to the foreland by the N–S-trending thrusts fronts.

The final stage of deformation (12.6 cm of shortening) is shown in Fig. 13a. The order of activation of the principal fault scarps is as follows: (1) the reactivated half-graben border, (2) the southern N–S-trending thrust, and (3) the northern N–S-trending thrust. This last scarp, perpendicular to the shortening direction, extends from the margin of the underlying half-graben and links with the pre-existing thrust front (2) to the south. An apparently continuous deformation front develops, even though both segments of the scarp are diachronous.

4.2.3. Contractional deformation stage. Comparison between different obliquity angles ($\alpha = 15°, 30°, 45°$)

The three models are compared in Fig. 14. After 2.5 cm of shortening, in the northwestern area, 15.8 cm of the half-graben length has been reactivated in Model 1 ($\alpha = 15°$); 12.3 cm in Model 2 ($\alpha = 30°$), and 9.5 cm in Model 3 ($\alpha = 45°$) respectively. This length decrease, observed also after 5.3 cm of shortening (Fig. 14), is an obvious consequence of the growing distance between the half-graben and the deformation front as α increases. Except for this difference, the evolution of the structure in Models 1 and 2 was similar to that described for Model 3. Partial reactivation of the oblique half-graben-bounding faults progressed from NW to SE during the early contractional stage, changing to a N–S trend as shortening progressed.

5. Discussion

5.1. Reactivation of the oblique half-graben

The analogue models presented in this paper and their comparison with the natural example provide templates for the understanding of contractional structures formed during progressive oblique shortening of a previous extensional basin and show additional aspects to those previously reported. In the models of Brun and Nalpas (1996) and Dubois et al. (2002), shortening is applied by displacement of a basal plate that ends directly beneath the half-graben, strongly influencing the deformation inside the half-graben. This experimental set-up promotes transpression and half-graben reactivation.

As in similar models presented by Panien et al. (2005) and Del Ventisette et al. (2006), our experimental results are less predetermined because the shortening is applied by displacement of the mobile wall, and both the hanging wall and the footwall are free to deform. The most striking feature found in our models as compared with those of the other authors is the significant development of contractional structures with normal-to-shortening strike directions, independent of the previous extensional

Author's personal copy

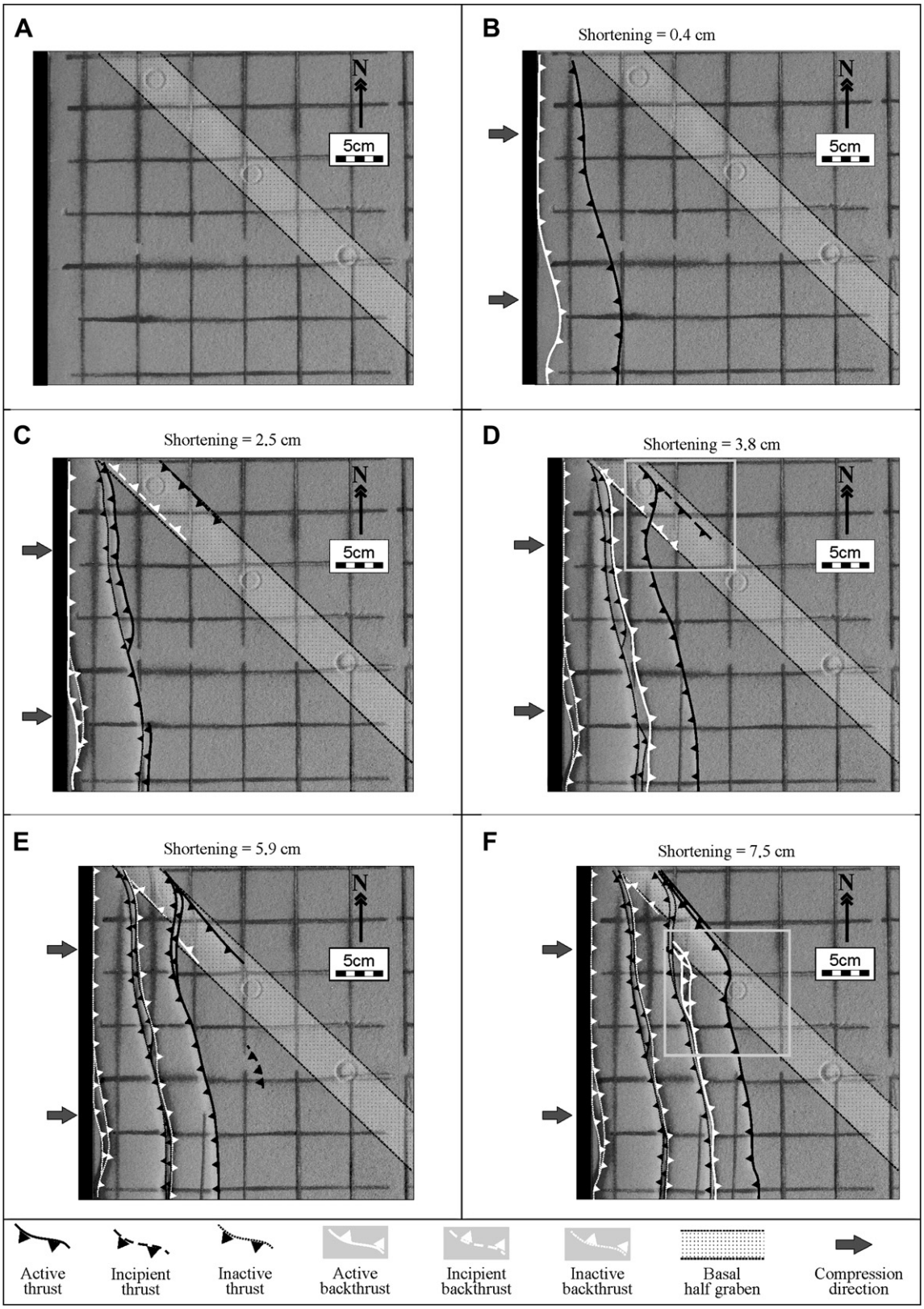

Fig. 12. Six stages of shortening of the inverted oblique half-graben (model 3, obliquity angle α of 45°). Photographs show plan views of the surface of the model. The fault pattern interpretation is shown at each step of progressive shortening. The dotted box marks the basal half-graben position. Black lines are reverse faults dipping to the left and white lines are reverse faults dipping to the right.

Author's personal copy

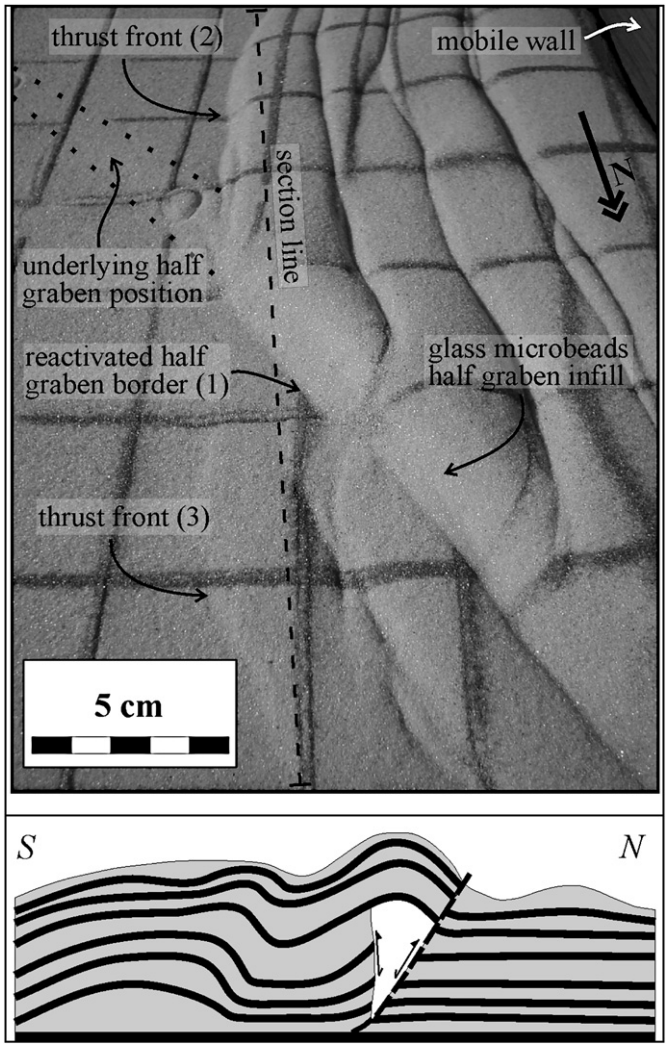

Fig. 13. (a) View to the south of the final deformation stage of the model. One can observe the differential uplift between the north and the south of the underlying half-graben. The numbers refer to the order of generation of each indicated fault scarp. The image also shows the location of the cross section of panel b. (b) Line drawing of the cross section generated by the GENERADOR.exe software. Vertical exaggeration = 3.5× (compare with Fig. 5).

structures. Moreover, in most of our experiments the normal master faults were not reactivated; instead, thrust faulting occurred inside the half-graben where weak microbeads with low coefficient of friction (Fig. 9) concentrated the deformation. The half-graben acts as a nucleation site for thrust faulting because of strong local competence contrasts.

Reactivation of the initial normal faults occurs only in mechanically favorable sectors of the system, where the half-graben is closer to the mobile wall (Fig. 14). As previous experiments have shown (e.g., Mulugeta, 1988), the spacing of imbricate thrusts is a function of the mechanical properties and thickness of the wedge material, as well as of the frictional resistance along the base. These parameters determine the propagation of the deformation front of a thrust system without basement controls. The oblique half-graben in our experiments introduces a N–S variation in boundary conditions, establishing two regions with different mechanical behavior. In the northern region, a segment of the oblique half-graben is reactivated and remains active during the entire experiment. In the southern region, the half-graben is further from the advancing wall. At some critical distance, the deformation front departs from the underlying control and becomes normal to the shortening direction. The extensional structures in the 'foreland' are not reactivated. Beyond this distance the effect of the basement structure can no longer mechanically affect the system (Nieuwland et al., 2000). As expected, the lengths of the reactivated segments of the half-graben decreases with growing obliquity angle α (Fig. 14b). At the final deformation stage a continuous front is left that obscures the oblique orientation of the reactivated extensional structures.

5.2. Limitations of the model

The two analogue materials used are, of course, an over-simplification of Earth deformation processes. For instance, we used only Coulomb materials that do not replicate viscous behavior. Moreover, the simple extensional structural pattern generated in the experiments does not truly represent a natural rift, which is obviously much more complex. However, these experiments allow us to gain first-order intuition into the influence of oblique half-graben configuration on the contractional reactivation process.

Interestingly, we observed that some of the extensional faults were not reactivated during inversion. This is most likely related to the physical properties of the modeling materials. Fault reactivation can occur under stress levels lower than those necessary to create new faults (Sibson, 1995), because pre-existing faults are surfaces along which the cohesive strength and the friction coefficient are lower than those of intact rock (Anderson, 1951). The sand used in the modeling has a low cohesive strength, so there is little difference between the strength of faulted and un-faulted sand. This insufficient contrast between faulted and un-faulted sand may facilitate the development of a new gently dipping reverse fault, rather than reactivate and rotate a pre-existing normal fault under contraction (Amilibia et al., 2005). This could explain why fewer than expected faults became reactivated during inversion. Other limitations of these experiments include neglect of pore fluid pressures, and the absence of thermal gradients with depth. Pore fluid pressure in particular may exert an important control on brittle fault reactivation (Sibson, 1985; Etheridge, 1986). Nevertheless, as was pointed by Panien et al. (2005), the use of weak microbeads with a low coefficient of friction (Fig. 9) as half-graben fill allowed the major half-graben-bounding faults to be reactivated.

5.3. Model versus nature

Although geometrical similarities found between structural maps do not, in themselves, imply similar deformation mechanisms, the fault styles and patterns of the Sierra Azul and our Model 3 strongly resemble each other and suggest the plausibility of similar deformational controls. Accordingly we make the following interpretations: (1) the N–S-trending thrust front of the Sierra Azul allows the eastern area of the structure to avoid reactivation (Fig. 7a) as described for the oblique rift model (Fig. 12), and (2) both the model structures and the Sierra Azul area show strong differential uplifts in north-south direction, with the southern block structurally higher then the northern one (compare Figs. 5 and 13b). Fig. 13 shows that deformation was concentrated in the southern section of the thrust system during the majority of the experiment. However, in the northern area, the thrust front overcame the basal weakness towards the foreland only during the final stages, thus achieving less structural uplift. This is a result of the obliquity of the half-graben with respect to the mobile wall.

The lack of access to more subsurface data between the two sections of Fig. 7 does not permit us to confirm whether the segments of the imaged half-graben bounding normal fault continue along strike and connect with the El Manzano–Liu Cullín lineament. Nevertheless the comparison with the experimental results highlights that the present geological setting can be explained assuming

Author's personal copy

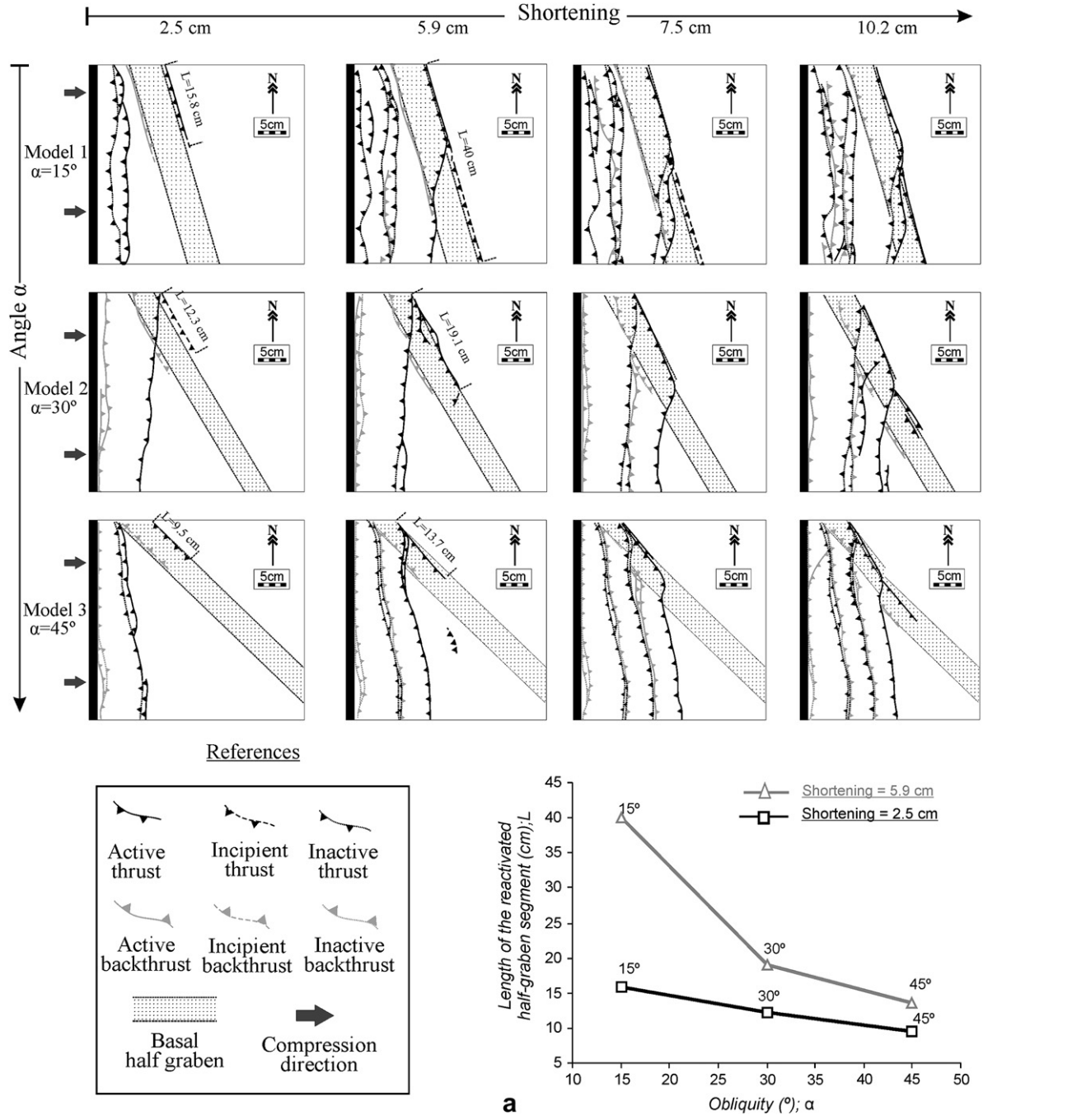

Fig. 14. Line drawings of top view of all models at different shortenings. The obliquity angles α (15°, 30° and 45°) increases along the *Y* axes, while the shortening applied (2.5 cm; 5.9 cm; 7.5 cm and 10.2 cm) increases along the *X* axes. For 2.5 cm and 5.9 cm of shortening, the value of *L* (length of the reactivated half-graben segment) is indicated. Plots of inset (a) shows the decrease of *L* with α for 5 cm and for 5.9 cm of shortening.

the presence of the oblique half-graben. Field and subsurface data suggest that the differential uplift between both margins of the El Manzano–Liu Cullín lineament arise from the reactivation of a Triassic–Jurassic half-graben border that could underlie the lineament (Figs. 2 and 5). Thicker deposits of Remoredo Formation cropping out to the south of the lineament indicate the location of the depocenter in good agreement with our suggestion. If this hypothesis is correct, the mainly N–S-trending axis of the Sierra Azul anticline may not reflect an underlying half-graben orientation, and may instead result from the loss of the control exerted by a NW–SE-trending half-graben over the deformation after its reactivation, as shown by the structural evolution of Model 3 (Fig. 12).

The proposed NW orientation of the half-graben is in agreement with the NE–SW extension developed in the Neuquén basin in the Triassic–Early Jurassic and later (Vergani et al., 1995; Cristallini et al., 2006) as well as with other narrow depocenters striking NNW–SSE across the Andes described in the northernmost part of the Malargue belt (Alvarez et al., 2000; Giambiagi et al., 2005).

6. Concluding remarks

Our sandbox experiments simulate the shortening of a half-graben previously developed during an extensional phase and filled

Author's personal copy

with weak glass microbeads. Despite the limitations of modeling techniques, the results of the oblique contraction process provide insights into the understanding and interpretation of inversion-related structures in nature as proposed for the southern Malargüe fold and thrust belt area.

The models results show that:

1. In most cases the normal master faults are not reactivated.
2. The microbeads infilling the half-graben act as nucleation sites for thrust faulting and control the location and orientation of the structures during inversion.
3. The contractional strain is initially accommodated by the reactivation of pre-existing half-graben segment closest to the deformation front. At some critical distance, the deformation front departs from the half-graben control and becomes normal to the shortening direction.
4. The resulting structural architecture preserves the extensional structures in the 'foreland' without reactivation.
5. The length of the reactivated segment of the half-graben decreases with growing obliquity angle α.

The results allow us to construct a three-step structural evolution: (i) reactivation of the proximal segment of the oblique half-graben; (ii) thrust front departure of the half-graben control, taking a normal-to-shortening strike; and (iii) generation of a continuous scarp through its propagation across the underlying weak zone.

Field and geophysical data of Sierra Azul area show:

1. Two uninverted Jurassic half-graben segments identified by well and seismic data to the east of the Sierra Azul.
2. Higher structural uplift and thicker Triassic-Jurassic syn-rift sequences to the south of the El Manzano–Liu Cullín lineament, indicating a possible depocenter border.
3. Strong alignment between the two normal faults identified by subsurface data and the restored position of the El Manzano–Liu Cullín lineament, suggesting that they were segments of a single structure prior to the Andean deformation.

Comparison with the experimental results highlights that the present geological setting can be explained with the presence of the proposed half-graben in the subsurface. If this hypothesis is correct, the deformation front (the mainly N–S-trending axis of the Sierra Azul anticline) crosses the underlying NW–SE-trending proposed structure, independent of the underlying half-graben orientation. In this interpretation, the El Manzano–Liu Cullín lineament would represent the superficial expression of an inverted NW–SE-trending half-graben. This orientation is in agreement with the NE–SW extension direction developed in the Neuquén basin in the Triassic–Early Jurassic.

The presented model could provide key information for delineating structural evolution and developing exploration strategies in this and other regions by helping to unravel the extensional architecture hidden by the inversion-related structures.

Acknowledgments

We wish to thank Repsol-YPF for authorization to publish borehole and seismic data. This study has been supported by CONICET (PIP 5758/05), UBA, Fundación Antorchas and Agencia Nacional de Promoción Científica y Técnica (PICT 38295). Special thanks to Ben Brooks and Phoebe Judge for their useful suggestions and comments. The editor J. Hippertt, and reviewers F. Hongn and F. Storti provided very useful comments that helped to substantially improve the manuscript.

References

Alvarez, P.P., Ramos, V.A., Giambiagi, L.B., Godoy, E., 2000. Relationships between different depocenters of Triassic–Jurassic rift systems in the Main Andes of Argentina and Chile. 23rd Geological International Congress, Proceedings on CD.

Amilibia, A., McClay, K.R., Sàbat, F., Muñoz, J.A., Roca, E., 2005. Analogue modeling of inverted oblique rift systems. Geological Acta 3, 251–271.

Anderson, E.M., 1951. The Dynamics of Faulting and Dyke Formation with Applications to Britain. Oliver and Boyd, Edinburgh. 191pp.

Brissón, I., Veiga, R., 1998. La estratigrafía y estructura de la Cuenca Neuquina. Gira de campo. Repsol YPF. Unpublished report, Buenos Aires, Argentina.

Brun, J.P., Nalpas, T., 1996. Graben inversion in nature and experiments. Tectonics 15, 677–687.

Burbank, D.W., Vergés, J., Muñoz, J.A., Bentham, P., 1992. Coeval hindward -and forward- imbricating thrusting in the South–Central Pyrenees, Spain; timing and rates of shortening and deposition. Geological Society of America Bulletin 104, 3–17.

Buchanan, P.G., McClay, K.R., 1991. Sandbox experiments of inverted listric and planar fault systems. Tectonophysics 188, 97–115.

Buchanan, P.G., McClay, K.R., 1992. Experiments on basin inversion above reactivated domino faults. Marine and Petroleum Geology 9, 486–500.

Byerlee, J., 1978. Friction of rocks. Pure and Applied Geophysics 116, 615–626.

Carrera, N., Muñoz, J.A., Sábat, F., Mon, R., Roca, E., 2006. The role of inversion tectonics in the structure of the Cordillera Oriental (NW Argentinean Andes). Journal of Structural Geology 28, 1921–1932.

Casas-Sainz, A.M., 1993. Oblique tectonic inversion and basement thrusting in the Cameros Massif (Northern Spain). Geodinamica Acta 6, 202–216.

Cristallini, E., Bottesi, G., Gavarrino, A., Rodríguez, L., Tomezzoli, R., Comeron, R., 2006. Synrift geometry of the Neuquén Basin in northeastern Neuquén Province, Argentina. In: Kay, S.M., Ramos, V.A. (Eds.), Evolution of an Andean Margin: A Tectonic and Magmatic View from the Andes to the Neuquén Basin (35°–39°S lat). Geological Society of America Special Paper, 407, pp. 147–161.

Dalziel, I., 1986. Collision and Cordilleran orogenesis: an Andean perspective. In: Coward, M.P., Ries, A.C. (Eds.), Collision Tectonics. Geological Society Special Publication, 19, pp. 389–404.

Del Ventisette, C., Montanari, D., Sani, F., Bonini, M., 2006. Basin inversion and fault reactivation in laboratory experiments. Journal of Structural Geology 28, 2067–2083.

Dessanti, R.N., 1973. Descripción geológica de la Hoja 29b Bardas Blancas (Provincia de Mendoza). Servicio Nacional Minero Geológico, Boletín 139.

Dicarlo, D., 2005. Estructura y Geología en la márgen Norte del Río Grande, Área de Bardas Blancas, Provincia de Mendoza. Tesis de Licenciatura, Facultad de Ciencias Exactas y Naturales Universidad de Buenos Aires.

Dimieri, L., 1997. Tectonic wedge geometry at Bardas Blancas, southern Andes (36°S), Argentina. Journal of Structural Geology 19 (11), 1419–1422.

Dubois, A., Odonne, F., Massonnat, G., Lebourg, T., Fabre, R., 2002. Analogue modeling of fault reactivation: tectonic inversion and oblique remobilisation of grabens. Journal of Structural Geology 24, 1741–1752.

Eisenstadt, G., Withjack, M.O., 1995. Estimating inversion: results from clay models. In: Buchanan, J.G.B., Buchanan, P.G. (Eds.), Basin Inversion. Geological Society Special Publication, 88, pp. 119–136.

Etheridge, M.A., 1986. On the reactivation of extensional fault systems. Philosophical Transactions of the Royal Society of London Series A: Mathematical and Physical Sciences 317, 179–194.

Fantín, J., 2006. Geología y Estructura del flanco oriental de la Sierra Azul y del Sinclinal de Quechuvil, Provincia de Mendoza. Tesis de Licenciatura, Facultad de Ciencias Exactas y Naturales Universidad de Buenos Aires.

Giambiagi, L., Alvarez, P.P., Bechis, F., Tunik, M., 2005. Influencia de las estructuras de rift triásico-jurásicas sobre el estilo de deformación de las fajas plegadas y corridas de Aconcagua y Malargüe, Mendoza. Revista de la Asociación Geológica Argentina 60 (4), 662–671.

Gillcrist, R., Coward, M., Mugnier, J.L., 1987. Structural inversion and its controls: examples from the Alpine foreland and the French Alps. Geodinamica Acta 1, 5–34.

Groeber, P., 1937. Mapa Geológico de la Hoja 30c (Puntilla del Huincan) del mapa Geológico General de la República Argentina. Dirección Nacional de Minería y Geología.

Groeber, P., 1980. Observaciones geológicas a lo largo del meridiano 70°. Asociación Geológica Argentina Serie C. Reimpresiones I, 1–174.

Gulisano, C., Gutierrez Pleimling, A., 1994. Field trips guidebook, Neuquina Basin. Mendoza Province. 4th International Congress on Jurassic Stratigraphy and Geology.

Hubbert, M.K., 1937. Theory of scale models as applied to the study of geologic structures. Geological Society of America Bulletin 48, 1459–1520.

Hubbert, M.K., 1951. Mechanical basis for certain familiar geologic structures. Geological Society of America Bulletin 62, 355–372.

Koopman, A., Speksnijder, A., Horsfield, W.T., 1987. Sandbox model studies of inversion tectonics. Tectonophysics 137, 379–388.

Kozlowski, E., Cruz, C., Condat, P., Manceda, R., 1989. Informe geológico zona Malargüe Occidental. YPF (Unpublished Report), Buenos Aires, Argentina.

Kozlowski, E., Manceda, R., Ramos, V., 1993. Estructura. In: Ramos, V. (Ed.), Geología y Recursos Naturales de Mendoza. Relatorio del XII Congreso Geológico Argentino y II Congreso de Exploración de Hidrocarburos, pp. 235–256.

Krantz, R.W., 1991. Measurements of friction coefficients and cohesion for faulting and fault reactivation in laboratory models using sand and sand mixtures. Tectonophysics 188, 203–207.

Author's personal copy

Legarreta, L., Gulisano, C.A., 1989. Análisis estratigráfico secuencial de la Cuenca Neuquina (Triásico superior–Terciario inferior), Argentina. In: Chebli, G., Spalletti, L. (Eds.), Cuencas Sedimentarias Argentinas: Serie Correlación Geológica, 6, pp. 221–243.

Legarreta, L., Uliana, M., 1991. Jurassic-Cretaceous marine oscillations and geometry of back-arc basin fill, central Argentine Andes. In: Macdonald, D.I.M. (Ed.), Sea-Level Changes at Active Plate Margins: Processes and Products. International Association of Sedimentologists Special Publication, 12, pp. 429–450.

Legarreta, L., Kokogian, D., Boggetti, D., 1985. Informe Sierra de Palauco. Estratigrafía. Provincia de Mendoza. YPF Unpublished report, Buenos Aires, Argentina.

Macedo, J., Marshak, S., 1999. Controls on the geometry of fold thrust belt salients. Geological Society of America Bulletin 111 (12), 1808–1822.

Manceda, R., Figueroa, D., 1993. La inversión del rift mesozoico en la faja fallada y plegada de Malargüe, Mendoza. XII Congreso Geológico Argentino, II Congreso de Exploración de Hidrocarburos (Buenos Aires). Actas III, 219–232.

Manceda, R., Figueroa, D., 1995. Inversion of the Mesozoic Neuquén Rift in the Malargüe Fold and Thrust Belt, Mendoza, Argentina. In: Tankard, A., Suárez, R., Welsink, H. (Eds.), Petroleum Basins of South America. American Association of Petroleum Geologists Memoir, 62, pp. 369–382.

McClay, K.R., 1989. Analogue models of inversion tectonics. In: Cooper, M.A., Williams, G.D. (Eds.), Inversion Tectonics. Geological Society Special Publication, 44, pp. 41–59.

McClay, K.R., Buchanan, P.G., 1992. Thrust faults in inverted extensional basins. In: McClay, K.R. (Ed.), Thrust Tectonics. Chapman and Hall, London, pp. 93–114.

McClay, K., Dooley, T., Ferguson, A., Poblet, J., 2000. Tectonic evolution of the Sanga Sanga block, Mahakam delta, Kalimantan, Indonesia. American Association of Petroleum Geologists Bulletin 84, 765–786.

Mingramm, A.R.G., Gonzalez Segura, J., Nocioni, A., 1993. Foldbelt tectonics of the Malargüe Area, Central West Argentina. XII Congreso Geológico Argentino, II Congreso de exploración de Hidrocarburos (Mendoza). Actas III, 179–187.

Mitra, S., Islam, Q.T., 1994. Experimental (clay) models of inversion structures. Tectonophysics 230, 211–222.

Mulugeta, G., 1988. Modelling the geometry of Coulomb thrust wedges. Journal of Structural Geology 10, 847–859.

Nieuwland, D.A., Leutscher, J.H., Gast, J., 2000. Wedge equilibrium in fold-and-thrust belts: prediction of out-of-sequence thrusting based on sandbox experiments and natural examples. Geologie en Mijnbouw/Netherlands Journal of Geosciences 79, 81–91.

Pángaro, F., Pereira, M., Giorgetti, M., 2004. Relevamiento Geológico del Precuyano en las Sierras de Reyes y Cara Cura, Provincia de Mendoza, Argentina. Repsol YPF. Unpublished report, Buenos Aires, Argentina.

Panien, M., Schreurs, G., Pfiffner, A., 2005. Sandbox experiments on basin inversion: testing the influence of basin orientation and basin fill. Journal of Structural Geology 27 (3), 433–445.

Quintana, A., 2008. Geología de la Sierra Azul (Departamento de Malargüe, Provincia de Mendoza). Tesis de Licenciatura, Facultad de Ciencias Exactas y Naturales Universidad de Buenos Aires.

Ramberg, H., 1981. Gravity, Deformation and the Earth's Crust, second ed. Academic Press, London.

Ramos, V.A., 1989. The birth of southern South America. American Scientist 77, 444–450.

Sandford, A.R., 1959. Analytical and experimental study of simple geologic structures. Geological Society of America Bulletin 70, 19–52.

Sibson, R.H., 1985. A note on fault reactivation. Journal of Structural Geology 7, 751–754.

Sibson, R.H., 1995. Selective fault reactivation during basin inversion: potential for fluid redistribution through fault-valve action. In: Buchanan, J.G., Buchanan, P.G. (Eds.), Bain Inversion. Geological Society of London, pp. 3–19. Special Publications 88.

Silvestro, J., Kraemer, P., 2005. Constraining the Neogene evolution of the Central Andes fold belt between 35°–36°S using top-wedge-growth strata record, Malargüe, Argentina. 6th International Symposium on Andean Geodynamics, Extended Abstracts, Barcelona, p. 670-672.

Uliana, M.A., Biddle, K.T., Cerdán, J., 1989. Mesozoic Extension and the Formation of Argentine Sedimentary Basins. In: Tankard, A.J., Balkwill, H.R. (Eds.), Extensional Tectonics and Stratigraphy of the North Atlantic Margins. American Association of Petroleum Geologists Memoir, 46, pp. 599–614.

Vergani, G.D., Tankard, A.J., Belotti, H.J., Welsink, H.J., 1995. Tectonic evolution and paleogeography of the Neuquén basin, Argentina. In: Tankard, A.J., Suárez, S.R., Welsink, H.J. (Eds.), Petroleum Basins of South America. American Association of Petroleum Geologists Memoir, 62, pp. 383–402.

Vergés, J., Muñoz, J.A., 1990. Thrust sequences in the Southern Central Pyrenees. Bulletin de la Société Géologique de France 8, 265–271.

Yagupsky, D.L., Cristallini, E.O., Zamora, G., Varadé, R., 2007. Sistema compresivo sobreimpuesto a un rift oblicuo: aplicaciones en la faja plegada y corrida de Malargüe, Sur de Mendoza. Revista de la Asociación Geológica Argentina 62 (I), 124–138.